

# The MOAO system of the IRMOS near-Infrared Multi-Object Spectrograph for TMT

David R. Andersen,<sup>a</sup> Stephen S. Eikenberry,<sup>b</sup> Murray Fletcher,<sup>a</sup> William Gardhouse,<sup>a</sup> Brian Leckie,<sup>a</sup> Jean-Pierre Véran,<sup>a</sup> Don Gavel,<sup>c</sup> Richard Clare,<sup>d</sup> Rafael Guzman,<sup>b</sup> Laurent Jolissaint,<sup>a</sup> Roger Julian,<sup>b</sup> William Rambold<sup>b</sup>

<sup>a</sup>NRC Herzberg Institute of Astrophysics, 5071 W. Saanich Rd., Victoria, BC, CANADA;

<sup>b</sup>Department of Astronomy, University of Florida, 211 Bryant Space Science Center, City, Country, P.O. Box 112055, Gainesville, FL, USA

<sup>c</sup>Center for Adaptive Optics, University of California, 1156 High St., Santa Cruz, CA, USA

<sup>d</sup>TMT Project Office, California Institute of Technology, 1200 E. California Blvd, Mail Code 102-8, Pasadena, CA, USA

## ABSTRACT

The near-Infrared Multi-Object Spectrograph (IRMOS) for TMT is one of the most powerful astronomical instruments ever envisioned. The combination of the collecting area of TMT, the unique image-sharpening capabilities of the Multi-Object Adaptive Optics (MOAO) system, and the multiplexing advantage of the multi-object integral-field spectra provided by the IRMOS back-end make it capable of addressing some of the leading scientific challenges of the coming decades. Here we present an overview of one potential IRMOS concept and then focus on the MOAO system. In particular we will describe our concept for the laser and natural guide star wavefront sensors, deformable mirrors and the calibration system of MOAO. For each of these design elements, we describe the key trade studies which help define each subsystem. From results of our studies, we assemble a MOAO ensquared energy budget. We find that 50% of the energy is ensquared within the 50 milli-arcsecond spatial pixel of the IRMOS integral field units for a wavelength of  $1.65\mu\text{m}$ . Given the requirements placed on the MOAO system to achieve this performance, large ensquared energies can be achieved with even finer plate scales for wavelengths longer than  $1.5\mu\text{m}$ .

**Keywords:**

## 1. INTRODUCTION

IRMOS is a Near-Infrared (NIR) integral-field Multi-Object Spectrograph (MOS) envisioned for the TMT. Each of the  $\sim 20$  scientific objects targeted by IRMOS will be corrected by Multi-Object Adaptive Optics (MOAO), making IRMOS both a very powerful and unique instrument concept. MOAO, in combination with the multiplex advantage of the MOS system, make IRMOS the ideal machine for settling some of the leading astronomical questions which the TMT is being built to address. Tracing the formation of galaxies at redshifts from  $1 < z < 6$ , along with identifying and studying the more distant first light objects in the Universe serve as the the guiding design reference science cases (DRCs) for the IRMOS feasibility study carried out at the University of Florida and the NRC Herzberg Institute of Astrophysics (HIA). The designs for the MOAO system, MOS probes, integral field units (IFUs) and spectrographs are optimized to meet the scientific requirements that flowed down from these DRCs.

The MOAO system, which is the focus of this paper, is required to deliver near diffraction-limited images to the  $\sim 2''$  IFUs situated throughout the five arcminute field of regard (FOR). Defining “near diffraction-limited” requires an examination of the spatial scales of the DRC targets. Based on the  $\sim 50$  milli-arcsecond (mas) diameter of  $z \sim 2$  star formation regions and the expected sizes of  $\sim 100\text{mas}$  of  $z \sim 10$  Ly $\alpha$  sources, the spatial resolution of IRMOS is chosen to be 50mas. Therefore, we translate “near diffraction limited imaging” into

---

Further author information: (Send correspondence to D.R.A.)  
E-mail: david.andersen@nrc-cnrc.gc.ca, Telephone: 1 250 363 8708

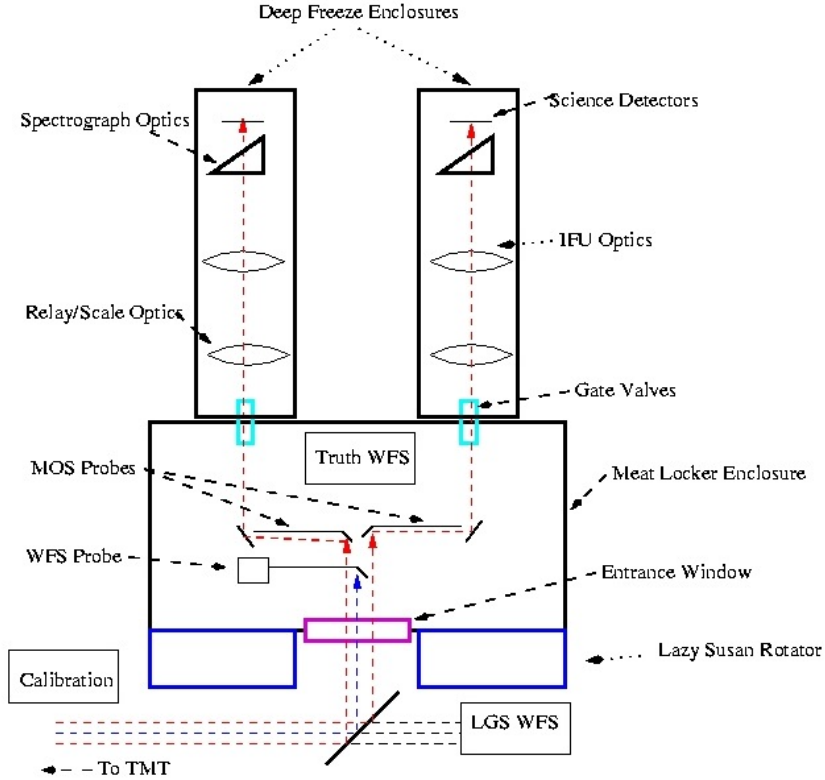


**Figure 1.** IRMOS schematic. The dichroic and LGS WFS system are located in the ambient environment. The “Meat-locker” is a vacuum cooled to  $-40^{\circ}\text{C}$  and contains the NGS WFS system, the MOS probe arms with embedded woofer-tweeter DMs, and the Truth WFS. Each MOS probe arm feeds light into a separate “Deep Freeze,” which is a cryogenic ( $\sim 80\text{K}$ ) environment containing the IFU image slicer, spectrograph optics and science detectors.

a requirement that the MOAO system ensquare 50% of the energy from a point spread function (PSF) at a wavelength of  $1.65\mu\text{m}$  into a  $50\text{mas}$  square\*. A second requirement which flows down from the DRCs is that IRMOS deliver this 50% ensquared energy (EE) within  $50\text{mas}$  almost anywhere on the sky — MOAO is required to provide 90% sky coverage at the galactic pole.

While there have been previous studies of MOAO,<sup>1</sup> a MOAO system capable of delivering the image quality requirements of IRMOS is novel. Therefore, in addition to designing the wavefront sensors (WFS) and describing the DMs, as presented in section 2, a great deal of the effort associated with this study focused on delivering an EE budget for the MOAO system (see also Gavel<sup>2</sup>). It should be emphasized that the EE budget, presented in section 3, naturally is split between high order errors which scatter light out of  $50\text{mas}$  — error terms such as actuator saturation and round-off errors — and low order errors which broaden the core of the point spread function (PSF) without necessarily lowering the EE within  $50\text{mas}$  — error terms such as tip-tilt and Seidel aberrations. By making this break, the limitations (and new possibilities) of the IRMOS MOAO system become apparent.

\*While requiring 50% EE within  $50\text{mas}$  at shorter wavelengths improves the scientific performance of IRMOS, achieving that goal involves a substantial increase in cost and risk, as we will show. If 50% of the EE is contained within  $50\text{mas}$  at  $1.65\mu\text{m}$ , IRMOS can successfully address the DRCs.

## 2. IRMOS MOAO DESIGN

### 2.1. Overview

In this section, we describe the design of the MOAO system as well as some of the the trade studies motivating the designs of different MOAO subsystems. We begin by providing an overview of the entire IRMOS concept (for more detail, see Eikenberry<sup>3</sup>), and then focus attention on individual components of the MOAO system.

IRMOS contains two basic operational systems: the MOAO system and a science backend for target selection and integral field spectroscopy (Figure 1). IRMOS, like all TMT instruments, is mounted on a Nasmyth platform and contains three primary volumes characterized by different operating temperatures: 1) The ambient temperature Laser Guide Star (LGS) WFS subsystem. 2) the meat locker, a vacuum volume near the TMT input focal plane with an operating temperature of  $\sim 230$  K containing the Natural Guide Star (NGS) WFSs and the MOS probe arms. The set of  $\sim 20$  fixed-optical-path  $2''$  FOV deployable MOS probe arms patrol a  $5'$  FOR. Each arm contains Atmospheric Dispersion Correctors (ADCs) and MOAO Deformable Mirrors (DMs) opto-mechanically embedded in the subsystem itself, providing integrated AO correction for the science path. 3) Finally the deep-freeze is separated from the meatlocker by gate valves, and is a vacuum volume operating at  $\sim 80$ K. The deep freeze contains the final re-imaging optics for the MOS pickoffs, the IFUs, and the spectrograph optics, mechanisms, and science detectors.

A photon from TMT directed towards IRMOS first encounters a large dichroic that directs light bluewards of 0.6 microns (especially light from the Sodium beacons) into the LGS WFS subsystem and light redwards of 0.8 microns into the meatlocker subsystem. Besides separating the beam, the dichroic also changes the optical axis of the meatlocker and spectrograph subsystems to a vertical orientation; a vertical optical axes allows the instrument to be de-rotated while maintaining a fixed gravitational axis. The TMT Laser Guide Star facility (LGSF)<sup>4</sup> will launch 8 Sodium beacons, light from which will be sensed and relayed to the TMT Real Time Controller (RTC)<sup>5</sup> The RTC will transform this signal into a tomographic model of the atmosphere above the observatory. If the photon from TMT has a wavelength longer than 0.8 microns, it will be directed up through a window and into the meatlocker. If the photon comes from a suitable star, it may be sensed by one of six NGS WFSs. These NGS WFSs also relay their WFS data to the RTC. Finally, if the photon has traveled from an interesting scientific target, it will be intercepted by one of the many MOS arms. It will be collimated, passed through an ADC corrected by a woofer-tweeter pair of DMs<sup>6,7</sup> and sent into the deep freeze. There, the photon will be refocused onto an image slicer and dispersed by a grating onto an infrared array.

Having taken a quick “tour” of IRMOS, we now focus on the elements of the design related to the IRMOS system. In each of the following subsections, we summarize the functions of the subsystem and important trade studies which informed the design. Finally, we present the design.

### 2.2. Laser Guide Star Wavefront Sensors

**Functionality:** The LGS WFS subsystem is responsible for providing all the high order WFS information required by the RTC to make a tomographic reconstruction of the atmosphere. This tomographic reconstruction of the turbulence above the observatory can be projected on the DMs in each of the MOS probe arms. The LGS WFSs must be usable at zenith angles down to  $60+$  degrees. This places a requirement that the conjugate height of the LGS WFS be adjustable between 85 and 210km. The LGSF will deliver 8 Sodium beacons: five, equispaced on a 5 arcminute diameter circle, and three equispaced on a 2.33 arcminute diameter circle.

**Trade Studies:** The central question relating the LGS design is determining the order to which the wavefront will be sensed. This question involves a trade between the two dominant terms in the error budget: tomographic and fitting errors. By comparing the tomographic and fitting errors for three field positions for both  $60\times 60$  and  $100\times 100$  subapertures, we made three discoveries. First, there is large variation in the tomographic errors across the FOV — from 77nm of wavefront error (WFE) at the center of the FOR to 167nm of WFE at the field edge for  $60\times 60$  subapertures. In addition, we found the that the median tomographic WFE for  $60\times 60$  subapertures was equal to the 108nm fitting error. Finally, we found that while the fitting error is substantially smaller for  $100\times 100$  subapertures (71nm vs. 108nm), this gain is partially offset by a larger tomographic error; high spatial frequency errors that previously were part of the fitting error become imperfectly-corrected tomographic errors (compare the median case where the tomographic error rose from 109nm to 124nm when using  $100\times 100$  versus

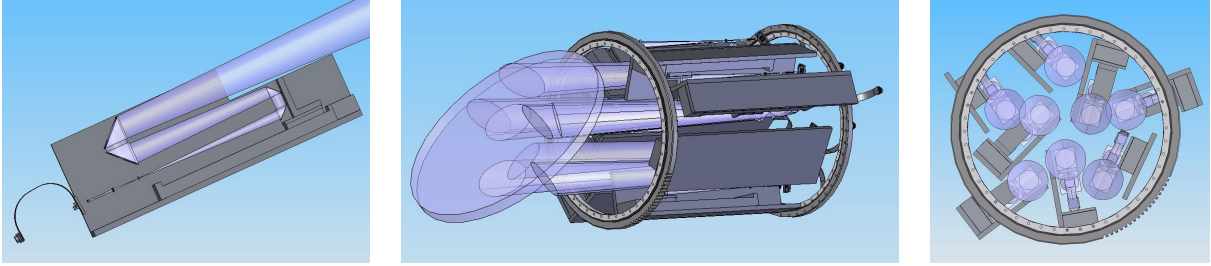


**Figure 2. Left Panel:** An individual LGS WFS trombone arm. As the distance to the Sodium layer increases with zenith angle, the trombone will shorten the optical path and keep the focus at the same point. **Central Panel:** Side view of the LGS WFS assembly. **Right Panel:** Face-on view of the LGS WFS assembly. This design would be difficult to modify if the density of LGS on sky were increased; the individual trombones are already tightly packed.

$60 \times 60$  subapertures). So while the total WFE of the  $100 \times 100$  subaperture system is smaller (142nm versus 153nm), this slight gain associated with increasing the number of subapertures is more than offset by greater costs and risks. The baseline design for the MOAO LGS WFS system therefore employs  $60 \times 60$  subapertures.

MOAO is the only currently envisioned astronomical implementation of AO that relies upon open loop control. Open loop control means that WFSs sense the whole WFE rather than a post-DM corrected residual WFE sensed by closed loop WFSs. Open loop control also implies that 1) non common path aberrations in the WFS will manifest themselves as WFEs in the science channel and 2) WFSs need to have higher dynamic ranges than their closed loop counterparts.

Without compensation, the LGS WFS will detect significant coma and astigmatism and introduce these non-common path aberrations into the MOAO corrected images. Left uncorrected, coma and astigmatism will lead to significant reductions in EE. However, because astigmatism is relatively constant and coma is predictable as the LGS WFS optical path changes length, the aberrations can be corrected by simple astigmatism and coma correctors in the individual LGS WFS arm. Coma and astigmatism are low order aberrations which is a distinct advantage when attempting to mitigate their effect. Because the figure of merit for the IRMOS MOAO system is EE within 50mas,  $\sim 100$ nm of coma or defocus can be tolerated with negligible ( $< 3\%$ ) loss of EE. Likewise, defocus, which will be introduced by variability in the altitude of the Sodium layer and may be as great as 150nm of WFE,<sup>8</sup> will decrease the EE within 50mas by less than 3%.

Because the LGS WFS operate in open loop; only tip-tilt is removed from the incoming beam by the fast steering mirrors of the LGSF. Therefore, the angle of arrival of the LGS spot will be highly variable and, it was worried, could lead to shortfalls in the dynamic range of the LGS WFS. We derived an analytical expression for the variance of the angle of arrival of the LGS spot images. We derived that the expected rms spot jitter at the focal plane of a LGS WFS sub-aperture will be  $\sim 40$ mas for  $r_0=15$ cm and a 0.5m subaperture spacing. MOAO will have a  $\sim 2.5$  margin if a matched filter algorithm for optimal centroiding is employed. A larger margin can be obtained by increasing the subaperture plate scale or using a different centroiding algorithm. We therefore believe the LGS WFS should have sufficient dynamic range to operate in open loop.

**Design:** As noted above, the LGS WFS subsystem is an ambient temperature/pressure system. It contains 8 separate wavefront sensor (WFS) assemblies (Figure 2). Each of the LGSs is assigned an optical trombone to compensate for the changing altitude of the sodium layer as a function of zenith distance (The slant range considered here is from 85 km to 210 km). The off-axis trombone assemblies are each tilted to have their motions pointed at the center of the telescope exit pupil. The steering mirrors can be mounted on a commercially available precision stage. After the trombone compensation, an in-focus image is presented at a fixed field stop. Following the field stop is a two-component zoom lens that provides a collimated beam for the lenslet array. A slight amount of zooming is required to maintain a constant beam patch size at the lenslet array due to the different focal distances for 85 and 210 km LGSs. The adjustment is for about a 3.3 per cent change in the size of the pupil patch. As noted above, a simple astigmatism corrector placed in the collimated beam before the lenslets corrects for much of the astigmatism generated by the dichroic beamsplitter and telescope. Likewise a second

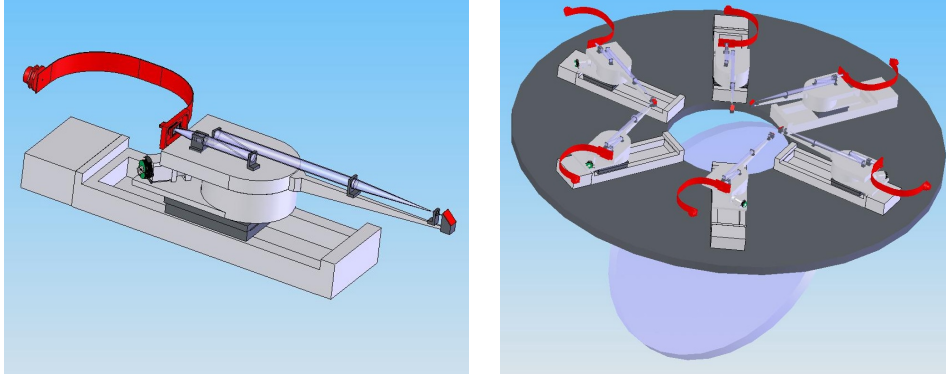


**Figure 3. Left Panel:** An individual NGS WFS probe arm. All of the optics and CCD are on a common mount and are rotated and moved together. **Right Panel:** The NGS WFS assembly. The six probe arms can each sweep out a large fraction of the FOR, giving the astronomer increased flexibility when selecting science and NGS targets.

corrector removes coma introduced by imaging a finite distance source off axis. Re-imaging optics transfer the spot pattern formed by the lenslets to a radial format CCD being developed by TMT.<sup>9</sup> A LGS WFS plate scale of  $0.5''$  per pixel is chosen.

Since the baseline design assumes the LGSs are fixed on sky, the LGS WFSs must de-rotate in the Nasmyth reference frame as the TMT tracks across the sky. The 8 assemblies are mounted in a tube that rotates at the same rate, tracking the LGS. The tube is mounted on a front/back pair of commercial slew bearings and driven by a backlash-free gear system.

To aid alignment and simplify maintenance, the 8 LGS assemblies will have identical optics and mechanical hardware. Each will be aligned in a jig so that the optics of all 8 assemblies are aligned to the same reference point. The 8 LGS assemblies are then installed in the tube and aligned to 8 sources representing the 8 laser guide stars. The sources are concentric to the virtual axis of the tube as defined by the slew bearings. The tube and its prime mover are then aligned on the telescope to the telescope's optic axis. Thus, in the unlikely event that some component on an assembly requires replacement, the part can be replaced, the assembly realigned in the jig, and then reinstalled in the tube without the need for night-time realignment to the laser guide star.

### 2.3. Natural Guide Star Wavefront Sensors

**Functionality:** The NGS WFS has four functions: 1) It is used to acquire the FOV in the presence of telescope pointing errors of order 1 arcsec rms. Therefore a NGS WFS FOV of 6 arcsec is required. 2) The NGS WFS produce measurements of focus which will be used by the RTC to compensate for rapid variations in the altitude of the Sodium layer which would otherwise introduce substantial defocus into the scientific images. 3) The multiple NGS WFSs are used to monitor and maintain the telescope-delivered plate scale. 4) Finally and most importantly, the NGS WFS will measure atmosphere tip-tilt and windshake which is corrected by the fast steering mirrors embedded in each MOS probe arm.

**Trade Studies** Given the functionality of the NGS WFS subsystem, the major trade associated with this subsystem is the determination of sky coverage. The general method used for determining sky coverage for the TMT facility NFIRAOS AO system is described in Clare et al.<sup>10</sup> We have adapted that method for IRMOS. The sky coverage model outputs the WFE variance due to atmospheric tip-tilt and telescope windshake taking into account a realistic distribution of NGS (based on Bahcall & Soneira<sup>11</sup> for the IRMOS modeling), and control bandwidth for a science fields located at the field center, and at radii of 1.25 and 2.5 arcminutes. Once again, we observe that the MOAO correction varies significantly over the field and is especially poor at the field edge. In general, however, the results are very promising and the results show 90% sky coverage is feasible because the errors, expressed in milli-arcseconds of tip-tilt are significantly smaller than 25mas. From a simulation using 4 NGS WFSs, a correction bandwidth of 20Hz, and 25mas of wind shake, we found that even at the field edge, the

EE within 50mas decreases by only 7% is negligible at all wavelengths for 90% sky coverage. EE losses are derived by convolving a simulated MOAO PSF with a Gaussian derived assuming 1 milliarcsecond of tip-tilt is equivalent to 36.4nm of tip-tilt WFE. While this analysis assumes that the tip-tilt error is azimuthally averaged (i.e. the Gaussian convolved with the image has no major axis), it is unlikely that a more realistic analysis would lead to significantly greater losses in ensquared energy. The MOAO design of IRMOS employs up to 6 tip-tilt focus stars and a tip-tilt bandwidth that can be substantially greater than 20 Hz. While these factors will presumably drive down the tip-tilt WFE further, we have already demonstrated that the IRMOS MOAO should have 90% sky coverage at the galactic poles.

**Design:** The NGS WFS subsystem consists of 6 identical WFS assemblies, each patrolling a wedge shape representing  $\sim 1/4$  of the FOV (Figure 3). This design is based closely on the successful On-Instrument Wavefront Sensor (OIWFS) designs for the Gemini Altair and FLAMINGOS-2 instruments,<sup>12</sup> using a pickoff mirror on the end of an arm. This approach can efficiently and flexibly patrol the available field with a position resolution of  $\sim 4$ mas. A high position resolution allows the NGS probes to make an accurate determination of the TMT delivered plate scale and allows the MOS probes to acquire faint science targets blindly. The resolution achieved in the design is more than required, but is easily achieved using a commercial gearing. Furthermore, since the IRMOS NGS system does not experience a changing gravity vector during use, the star will not move on the detector due to arm flexure.

The first optical element in the path is a converter lens which modifies the f/ratio of the beam slightly to shorten the overall length of the NGS WFS probe. A fold mirror, a 6" field stop, and a field lens follow the first element. After the collimator are two flats. A pupil is formed on this mirror and a slightly blurred pupil is formed on the first flat. The next optical elements are a 2x2 lens array and the first and second doublets of a re-imager. The CCD terminates the optical path where four images of the guide star appear. A commercially available CCD, such as EEV CCD60, would meet all requirements. The CCD 60 has a pixel size of 24 microns and the array format is 128x128. The image scale at the CCD is currently 0.10 arcseconds per pixel and the FOV for each lenslet is 6.0 arcsec.

Simply patrolling around the field in a plane means that the direction to the telescope exit pupil appears to change — an effect we call pupil wander. A consequence of this is the pupil patch at the lenslet array will be slightly displaced. For a 2x2 array, this results in the four stellar images having slightly disparate relative brightnesses. At the edge of the IRMOS field the mismatch is about 20% of the pupil patch radius. This causes the ratio of the faintest spot to brightest to be about 0.5. This will degrade the NGS WFS performance when working near the magnitude limit of the NGS WFS (which is likely to be a common occurrence). Design solutions exist which result in the pupil patch being stationary for all positions in the patrol field, but the drawback is that the WFS probe would vignette substantially more of the patrol field, thereby placing tighter restrictions on science target acquisition. A partial solution to address the IRMOS pupil wander problem is to tilt the linear stage to give a compromise pointing. The tilt would be about 0.2° for a probe location halfway to the edge of the field. The probe fold mirror would also have to be adjusted to point the optical axis to the center of the telescope exit pupil. This would give zero pointing error in the region of the center of the patrol area and deviating slightly elsewhere. The result would be pupil patch shifts of about 10% of the pupil radius instead of about 20%. For a 10% shift, the ratio of faintest spot to brightest is 0.7, greatly reducing the impact on WFS performance.

Each NGS WFS arm is mounted to a rotating platform which carries the complete optics package for that sensor. Mounting the optics package on the rotating stage makes the optics package and its alignment simple. The complete NGS WFS assembly bolts to an extension of the meat locker shaft for the azimuth bearing. The sweeping arm is moved radially on a commercially available precision linear stage. The long, thin pickoff arms and their pickoff mirrors intrude on the IRMOS FOR to select NGS targets. The arms have the ability to sweep into the area of their neighbors. Although this creates a redundancy for each sweep area and creates the need for absolute position tracking of both the rotating and translating assembly to prevent collisions, this design allows greater flexibility in the acquisition of NGS and should improve the efficiency of science target acquisition with the MOS probes. The pickoff arms patrol at a distance of 50mm in front of the focal surface. At this height, each pickoff arm projects a maximum area of 5747 mm square onto the focal surface when fully extended into the field of regard. This represents a vignetting of the focal surface of <1.7% per pickoff arm or <10.2% in total.

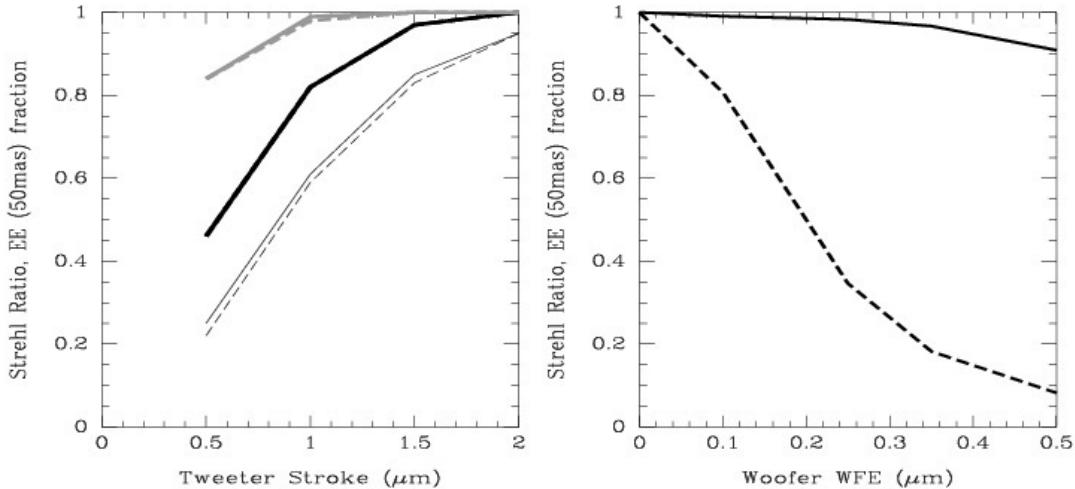


**Figure 4. Left Panel:** EE fraction within 50mas (solid lines) and Strehl ratio (dashed lines) versus the tweeter DM stroke threshold for three woofer DMs: a 19 actuator bimorph (thin lines), 36 actuator bimorph (heavy lines), and a 104 actuator bimorph DM (heavy grey lines). For a high order error like clipping due to DM saturation, EE and Strehl ratio are highly correlated. **Right Panel:** EE fraction within 50mas (solid line) and Strehl ratio (dashed line) versus woofer WFE induced by an imperfect hysteresis correction for a 36 actuator bimorph mirror and a large stroke tweeter DM. The woofer WFE is a low order error, and as such broadens the PSF without scattering significant light outside of 50mas. While the Strehl ratio declines rapidly with increasing WFE, the EE within 50mas remains high. Therefore, the IRMOS MOAO system can tolerate relatively large woofer errors, and does not necessarily need interferometers to monitor each woofer DM.

Because of the configurability of the NGS pickoff arms, this is a worst case scenario with the effective vignetting being much less — typically 5%.

## 2.4. Deformable Mirrors

**Functionality:** The MOAO correction is made by the woofer-tweeter pair of DMs embedded in each MOS probe arm. It is anticipated that the tweeter will be a high order MEMS mirror. Since it is unlikely that MEMS mirrors will be developed with sufficient actuator density and stroke to correct the entire wavefront, woofers are also required. Small, commercially available bimorph mirrors, for example, suffice.

**Trades:** In the process of evaluating the requirements on the woofer and tweeter, we performed two trade studies which clarified the requirements on both devices.

First, we assessed the effect of limited actuator stroke on the AO corrected image. We modeled a woofer-tweeter DM configuration with a curvature (bimorph) woofer. We simulated realizations of a random Kolmogorov phase screen. We had the woofer perfectly correct for tip and tilt plus the best fit to 19, 36 or 104 actuator curvature (bimorph) mirrors. For each case, we compute the reduction in Strehl ratio of the PSF and EE in a 50 mas pixel (Figure 4). We note that the EE and SR loss are almost identical. This means that saturated actuators on the tweeter DM takes energy from the core of the PSF and scatters it outside a 50 mas square pixel, i.e. it is lost from the point of view of the IRMOS IFU pixel. We conclude that a woofer with roughly 30 actuators is sufficient if the MEMS tweeter mirrors have 1.5 microns of stroke (which is realized by the current generation of high order 30×30 MEMS mirror). An advantage of these bimorph mirrors with 30 actuators is that they are readily available from commercial vendors and do not present either a great technical or cost risk.

Gavel<sup>2</sup> reports that MEMS mirrors show almost no hysteresis and need to be recalibrated only rarely. Bimorph mirrors, which we propose to use as woofers in each arm, do suffer from hysteresis. Our second trade study was aimed at assessing at what level errors on the woofer introduced by an imperfect correction of hysteresis can

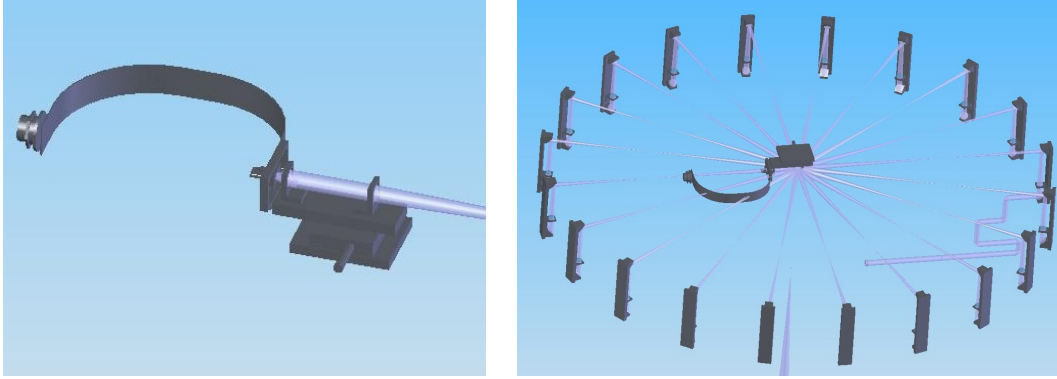


**Figure 5. Left Panel:** The WFS is mounted to a high precision rotation stage that can point the WFS toward any one of the  $\sim 20$  MOS probe arms. **Right Panel:** Orientation of TWFS with respect to the optical path of the MOS probe arms. Light from the selected MOS probe will be picked off and directed towards the TWFS during observations in order to sense telescope flexure (instrument flexure should be small during observations).

be tolerated. If the tolerance on woofer-induced WFE was high, constant monitoring of the woofer by an interferometer would be required. Using a similar approach as described above, we measured EE and Strehl ratio of images with various amounts of woofer surface error (the tweeter for this simulation was limited to a 2 micron stroke) (Figure 4). The loss in Strehl Ratio and ensquared energy due to errors on the woofer were not correlated. Errors on the shape of the woofer remove light from the central core of an Airy PSF and broaden that core. Therefore, as these lower order wavefront errors increase, the Strehl ratio drops, but most of the light remains within 50 mas. For IRMOS, the implication is that we do not need to monitor the woofer DMs with interferometers if only a 50mas IFU pixel is considered.

**Description** The woofer DM for IRMOS is baselined as a 31-actuator CILAS BIM31 bimorph mirror. The 31 actuators are distributed in 4 rings with 1, 6, 12 and 12 actuators in each ring. The bimorph mirror has a full mechanical stroke of 20 microns of defocus when  $\pm 400V$  is placed on the electrodes. Hysteresis is  $<6\%$  for a  $\pm 400V$  cycle. The useful optical aperture is 50-55mm. The CILAS bimorph active area of  $\sim 50$ -mm in diameter is a very close match to the 46-mm diameter produced by the MOS collimator lens here. Once a final woofer selection is made for IRMOS, the collimator focal length and location can easily be tweaked to provide an even closer match between the beam size and DM active area. Alternatively, custom bimorph mirrors are available from CILAS with more actuators packed in a smaller area (with a trade off on the total stroke). The CILAS bimorph mirrors can operate in vacuum and have been tested down to  $-10^\circ C$ . While the mirrors need to be tested at  $-40^\circ C$ , there is no fundamental reason they should not work at this temperature.

The tweeter DM for IRMOS is baselined as a  $60 \times 60$ -actuator MEMS deformable mirror. Based on the MOAO trade studies described above, we require a MEMS mirror with at least 1.5 microns of stroke. The Gemini GPI instrument,<sup>13</sup> which is entering its Preliminary Design Phase in early 2006, requires a  $60 \times 60$  DMs with identical stroke requirements to the IRMOS tweeters five years before IRMOS will, and is currently funding the development of these DMs at Boston Micromachines. This effort provides some risk mitigation for acquiring  $60 \times 60$ -actuator MEMS DMs for IRMOS.

## 2.5. Calibration Systems

**Functionality:** The AO calibration system and the Truth WFS (TWFS) of IRMOS are the final two elements of the MOAO system. The calibration unit contains simulated NGS and LGS sources which will be used to characterize LGS and NGS WFS behavior and to monitor and flatten the DMs. As a goal, this unit will measure non-common path aberrations between the LGS WFS and science paths, improve alignment between the LGS subsystem and science rotation axes and establish DM to WFS influence functions.

The TWFS is located in the meat locker and senses light after it has passed through the MOS probe arms (including the DMs). Light from any of the MOS probes can be directed towards a central station where the

TWFS will be located. This WFS will contain a high order ( $60\times 60$ ) SH WFS feeding a CCD. The TWFS will be used to: 1) Measure and correct non-common path differences induced by flexure between the LGS system and the MOS probes during science observations. 2) Flatten the DMs during setup. 3) Monitor the MOAO-corrected image quality during operation. 4) Provide useful data relating to the quality of the MOAO tomography that will be useful when post-processing the scientific data.

**Description:** The calibration subsystem will be located in a housing separate from IRMOS which can be slid into place between IRMOS and the edge of the Nasmyth platform. Calibration Unit optics will simulate the converging  $f/15$  TMT beam. The LGS sources in the calibration unit are required to be conjugate to a single altitude between 85 and 210 with a goal to have an adjustable conjugate altitude between these extremes. The LGS source has to emit sufficient light at 589nm to calibrate the LGS WFS in a short period of time. At least two LGS sources are required, one to feed each ring of LGS WFSs. At least one NGS calibration source is required. Ideally, both NGS and LGS sources can be placed behind the same foreoptics so that a turbulence generator can be included so that IRMOS can be run closed loop during integration and testing.

The TWFS is located on the telescope axis inside the Meatlocker downstream of the focus and MOS probe arms. The Truth WFS subsystem consists of a rotating wavefront sensor and set of centering flip mirrors for each MOS probe. A flip mirror can intercept light from a MOS probe just before it enters a deep freeze dewar, deflecting the beam to the TWFS optics (Figure 5). Following the pickoff mirror are a pupil re-imaging lens, two fold mirrors, the WFS collimator, lenslet array, re-imager and CCD. The pupil re-imager mainly confines the beam to a manageable size when it reaches the WFS. The WFS itself is located at the center of the MOS subsystem, above the MOS probe patrol plane, and can be mounted on a commercially available precision rotary stage with the necessary resolution, accuracy, wobble and speed. The pupil re-imager and the TWFS collimator form an image of the telescope exit pupil on the lenslet array. The re-imager lens then shrinks the images from the lenslet array to fit onto the CCD. The beam patch is of sufficient size to fill a  $60\times 60$  Shack-Hartmann lenslet array. A low noise  $1000\times 1000$  EEV CCD201 can be used with a 100mas plate scale.

### 3. MOAO ERROR BUDGET

Creating an ensquared energy budget requires a slightly different approach than is traditional for AO systems because the driving requirement is on EE not wavefront error. The error budget has to be broken into high order and low order errors. High order errors, listed in Table 1, do not broaden the PSF but do reduce the Strehl ratio and throw light from the core out to large radii. Therefore, the EE within a relatively small aperture will match the Strehl ratio. Low order errors listed in Table 2, in contrast, will broaden the core of the PSF, but may not move light outside of the aperture of interest.

As we pointed out in section 2.1, the fitting and tomographic errors are roughly comparable and are the two dominant terms in the high order WFE budget. Low order errors, on the other hand, like tip-tilt, focus, astigmatism and coma have minimal impact on the ensquared energy performance with a 50mas aperture. Based on this EE error budget for a 50mas aperture, the MOAO performance of the IRMOS baseline delivers 50% EE within 50mas at a wavelength of  $1.65\mu\text{m}$ . There are some trades that can be made to improve the EE, but it may be difficult without significantly increasing the laser power and number of beacons produced by the LGS facility or decreasing the FOR.

Several potential IRMOS science cases called for spatial sampling finer than 50mas in order to work in crowded fields or study stellar populations in nearby (Virgo cluster!) galaxies. Because the high order error budget drives the imaging performance of IRMOS, MOAO should be capable of delivering diffraction-limited performance in H and K-bands with low to moderate Strehl ratios. Relatively minor changes in the MOAO system (adding interferometers into the MOS probe arms to monitor woofer hysteresis) and the IRMOS scientific backend<sup>3</sup> can make new and exciting science with IRMOS possible without sacrificing the ability to complete the DRC programs.

### 4. SUMMARY

MOAO is a novel AO technique which attempts to provide good AO correction in multiple directions within a relatively large FOR. Given the relative lack of experience in the astronomical community with MOAO systems,

**Table 1.** MOAO high order error budget. WFE are listed in units of nm rms. We define a best, worst and median case from LAOS simulations of 13 field positions. All simulations used the a 7 layer turbulence profile with  $r_0=15\text{cm}$  at  $0.5\mu\text{m}$  and  $d_0=50\text{cm}$  ( $60\times 60$  subapertures). A WFE is derived using the assumption that Strehl ratio is equal to EE for high order errors. Other terms in the error budget which carry the NFIRAOS note are taken from the latest NFIRAOS error budget.<sup>15</sup> We arrive at the total WFE by taking the quadrature sum of each of the individual terms.

Error Terms	Wavefront Error (nm)			Notes
	Best	Median	Worst	
Fitting Error	108	108	108	$\sigma^2 = 0.25(d_0/r_0)^{5/3}$
Tomography	77	109	167	LAOS <sup>14</sup> simulations
LGS Noise	30	30	30	NEA= 1''
MEMS Saturation	30	30	30	Woofers-Tweeters Trade Study
Telescope Aberrations	45	45	45	NFIRAOS
LGS Centroiding	20	20	20	TMT study <sup>16</sup>
Servo Lag	20	20	20	NFIRAOS
RTC Roundoff	20	20	20	NFIRAOS
WFS Optics	20	20	20	Design Requirement
Pupil Misregistration	60	60	60	Design Requirement (0.1 subaperture)
Contingency	35	35	35	
Total	168	185	224	

**Table 2.** MOAO low order error budget. The first term is the Strehl ratio imported from the high order error budget (Table 1) calculated for 3 scientific wavelengths. The intrinsic width of the PSF leads to a significant reduction in the EE measured within 50mas, especially at longer wavelengths. We therefore convolve the LAOS PSF with the broadening due to the tip-tilt errors. Tip-tilt errors are generated assuming 4 NGSs correct tip-tilt at 20Hz for 90% sky coverage. Most of the EE loss we list under Tip-Tilt is actually due to the energy distribution of the diffraction-limited PSF and is therefore unavoidable. The other errors in this list are low order terms that can potentially broaden the core of the PSF substantially, but do not scatter significant light outside 50 mas. The EEs quoted here are all ratios of EE due to aberrations versus the EE of the perfect diffraction-limited PSF. Woofer hysteresis can be eliminated if the woofer DM is monitored by an interferometer. We arrive at the total EE fraction by multiplying all of the terms together.

Error Terms	$\lambda$	EE Fraction (50mas)			Notes
		Best	Median	Worst	
High Order (Table 1)	$1.00\mu\text{m}$	0.33	0.26	0.14	Using EE=SR (high order)
	$1.65\mu\text{m}$	0.66	0.61	0.48	
	$2.20\mu\text{m}$	0.79	0.76	0.66	
Tip-Tilt	$1.00\mu\text{m}$	0.94	0.94	0.89	4 TT stars, 20Hz, 90% Sky Coverage
	$1.65\mu\text{m}$	0.91	0.90	0.86	
	$2.20\mu\text{m}$	0.84	0.83	0.79	
Woofers Hysteresis		0.98	0.98	0.98	Woofers-Tweeters Trade Study
Seidel Aberrations		1.00	0.99	0.98	Defocus, <sup>8</sup> Astigmatism & Coma
Total	$1.00\mu\text{m}$	0.30	0.24	0.13	
	$1.65\mu\text{m}$	0.59	0.53	0.40	
	$2.20\mu\text{m}$	0.65	0.61	0.50	

there remain many practical aspects of MOAO which need to be tested and developed. In particular, more work demonstrating the feasibility of open loop control and the development of appropriate MEMS mirrors and radial format CCDs are required before the IRMOS MOAO system can be built. However, we believe that on a 8–10 year timescale each of these challenges can and will be met.

In this paper, we have presented designs of the IRMOS MOAO system for TMT (Figure 6). The MOAO

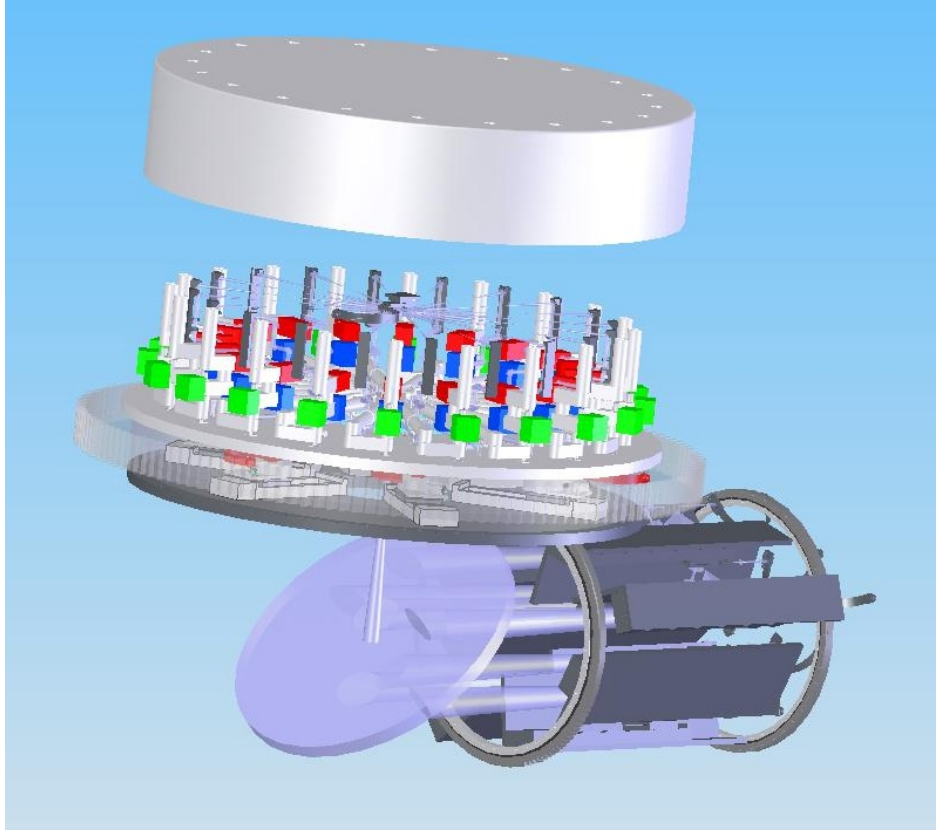


**Figure 6.** A view of all the MOAO components of IRMOS. The LGS WFS are located behind the dichroic. The NGS WFS are located just upstream of (below) the focal plane. The MOS probe arms contain the woofer and tweeter DMs. Finally, the TWFS can monitor the MOAO correction from one MOS probe arm. The NGS WFS, MOS probe arms and TWFS all reside in the Meatlocker.

system is highly distributed, existing in different volumes and operating in open loop. To mitigate the risks inherent in the design of an MOAO system, we have made design choices to reduce the complexity and the number of high risk components. Outside of the MEMS DMs (required by the Gemini Planet Imager on a shorter timescale) and radial format CCDs (required by most TMT AO systems), the MOAO design could be fabricated today.

We have also used simulations of MOAO, sky coverage and woofer-tweeter DMs to guide the design choices. Among the many results of this study, we highlight the following:

- LAOS MOAO simulations made clear that the gain of moving from a  $60 \times 60$  subaperture system to a  $100 \times 100$  subaperture system is slight and is offset by the greater risks associated with developing even higher order MEMS and radial format CCDs and the costs of these products.

- For high order WFE such as DM saturation, the loss in Strehl ratio is equivalent to losses in EE for a 50mas pixel. Low order wavefront errors, such as tip-tilt and astigmatism, significantly reduce the Strehl ratio but do not lead to large losses of EE within a 50mas aperture. Most of the low order errors do not produce significant EE losses.

- Because of the relaxed requirements on low order errors, 90% sky coverage can be achieved by the MOAO system with little or no loss (<4% median reduction) in EE.

- The rms spot jitter on the LGS WFS CCD will be less than 42.4mas. This provides a margin of 2.5 in the dynamic range of the LGS WFS CCD. This margin can be increased by using different centroiding algorithms

or adopting a larger plate scale.

- The MOAO tomographic performance will vary significantly across the FOR; the performance at the field edge shows an especially significant drop. A similar performance drop at the field edge is observed in the sky coverage simulations.

- Assuming the tweeter MEMS DMs have a 1.5 micron stroke, a  $\sim 36$  actuator bimorph mirror is sufficient to act as a woofer.

The over-arching goal of these trade studies is to help define the MOAO EE error budget. Using our baseline design, we have shown that 50% EE within 50mas can be achieved at a wavelength of  $1.65\mu\text{m}$ . Significantly increasing the EE will prove difficult; the density of LGSs would need to be significantly increased to drive down the tomographic error. Making this change would have multiple implications: 1) A new LGS WFS design would be required; 2) higher order DMs and WFSs would be required to prevent fitting error from being the dominant term in the EE budget; and 3) more laser power would be required to keep the LGS noise low. While these changes require significant increases in cost and risk to IRMOS, the error budget also made clear that the MOAO system should be able to deliver diffraction limited imaging in the  $H$  and  $K$ -bands. Relatively minor changes, such as adding interferometers to the MOS probe arms to monitor the woofers, would enable exciting new science beyond the scope of the original DRCs without sacrificing the performance of the MOAO system for the original plate scale. By delivering superior performance for multiple plate scales, IRMOS coupled to the MOAO system will be a powerful scientific workhorse for TMT.

## REFERENCES

1. Hammer, F. et al. 2004, SPIE, 5382, 727.
2. Gavel, D. et al. 2006, SPIE, *this conference* [6272-25].
3. Eikenberry, S.E. et al. 2006, SPIE *this conference* [6269-218].
4. R.R. Joyce, et al. 2006, SPIE *this conference* [6272-51].
5. Boyer, C. et al. 2006, SPIE *this conference* [6272-35].
6. Conan, R. et al 2006, SPIE *this conference* [6272-64].
7. Véran, J.-P. & Herriot, G. 2006, SPIE *this conference* [6272-48].
8. Herriot, G. & Hickson, P. 2006, SPIE *this conference* [6272-52].
9. Adkins, S.M., Zaucena, O., Nelson, J.E. 2006, SPIE *this conference* [6272-60].
10. Clare, R.M. et al. 2006, SPIE *this conference* [6272-107].
11. Bahcall, J.N., Soneira, R.M., 1980, *ApJ Supplement*, 44, 73.
12. Leckie, B.M. et al. 2006, SPIE *this conference* [6269-152].
13. Macintosh, B.A. et al. 2006, SPIE *this conference* [6272-20].
14. Ellerbroek, B.L., Gilles, L., Vogel, K. 2003, *Applied Optics*, 42, 4811.
15. Herriot, G. 2006, SPIE *this conference* [6272-24].
16. Gilles, L. & Ellerbroek, B.K. 2006, SPIE *this conference* [6272-57].